UCSF
UC San Francisco Previously Published Works

Title
The effect of simulated microgravity on lumbar spine biomechanics: an in vitro study

Permalink
https://escholarship.org/uc/item/2xq5q4zg

Journal
European Spine Journal, 25(9)

ISSN
0940-6719

Authors
Laws, Cory J
Berg-Johansen, Britta
Hargens, Alan R
et al.

Publication Date
2016-09-01

DOI
10.1007/s00586-015-4221-6

Peer reviewed

eScholarship.org Powered by the California Digital Library
University of California

Author Manuscript

Author Manuscript

Author Manuscript

Author Manuscript

HHS Public Access

Author manuscript

Eur Spine J. Author manuscript; available in PMC 2017 September 01.

Published in final edited form as:

Eur Spine J. 2016 September ; 25(9): 2889–2897. doi:10.1007/s00586-015-4221-6.

The effect of simulated microgravity on lumbar spine biomechanics: an in vitro study

Cory J. Laws[1], **Britta Berg-Johansen**[1], **Alan R. Hargens**[2], and **Jeffrey C. Lotz**[1]

[1] University of California, Box 0514, 513 Parnassus Avenue, Medical Sciences Bldg., San Francisco, CA 94143-0514, USA

[2] UCSD Medical Center, University of California, 350 Dickinson St., Suite 121, Mail Code 8894, San Diego, CA 92103-8894, USA

Abstract

Purpose—Disc herniation risk is quadrupled following spaceflight. This study tested the hypothesis that swelling-induced disc height increases (comparable to those reported in spaceflight) stiffen the spine and elevate annular strain and nuclear pressure during forward bending.

Methods—Eight human lumbar motion segments were secured to custom-designed testing jigs and subjected to baseline flexion and compression and pure moment flexibility tests. Discs were then free-swelled in saline to varying supraphysiologic heights consistent with prolonged weightlessness and re-tested to assess biomechanical changes.

Results—Swelling-induced disc height changes correlated positively with intradiscal pressure ($p < 0.01$) and stiffening in flexion ($p < 0.01$), and negatively with flexion range of motion ($p < 0.05$). Swelling-induced increases in disc height also led to increased annular surface strain under combined flexion with compression. Disc wedge angle decreased with swelling ($p < 0.05$); this loss of wedge angle correlated with decreased flexion range of motion ($R^2 = 0.94$, $p < 0.0001$) and decreased stiffness fold change in extension ($p < 0.05$).

Conclusion—Swelling-induced increases in disc height decrease flexibility and increase annular strain and nuclear pressure during forward bending. These changes, in combination with the measured loss of lordotic curvature with disc swelling, may contribute toward increased herniation risk. This is consistent with clinical observations of increased disc herniation rates after microgravity exposure and may provide the basis for future countermeasure development.

Keywords

Spaceflight; Microgravity; Intervertebral disc; Herniation; Biomechanics

Jeffrey C. Lotz lotzj@orthosurg.ucsf.edu.

Compliance with ethical standards

Conflict of interest The authors do not have any financial relationship with the organization that sponsored the research (NASA), and have full control of all primary data that the journal is free to review if requested.

Author Manuscript Author Manuscript Author Manuscript Author Manuscript

Introduction

Astronauts experience a 4.3-fold increase in herniated nucleus pulposus (HNP) incidence following spaceflight despite preventative measures and ongoing research [1]. HNP occurs when the annulus is overloaded in tension as the spinal motion segment is flexed while being compressed, and pressure forces nuclear material entirely or partially through the damaged region, most commonly the posterolateral annulus [2]. HNP often results in debilitating pain, and ultimately may require surgery. While many conditions can cause HNP via a multitude of mechanisms, the clinical experience implicates spinal flexion movements, while most in vitro reproductions in cadavers require a combination of compression plus flexion [3–5].

A plausible biomechanical mechanism of increased HNP risk post-spaceflight is as follows: lack of gravity reduces spinal loading and causes intervertebral discs to swell, increasing pressure in the nucleus pulposus and tension in the annulus fibrosus, thereby elevating HNP risk during spinal movements when gravity loading is restored. This premise is supported by observations that reduced spinal compression during bed rest causes increases in disc water content of about 10 %, leading to increased disc height and swelling [6]. This swelling increases the disc's resistance to bending and decreases the spine's range of motion (ROM), and is thought to increase the risk of injury in the early morning [7]. Spinal unloading and disc swelling persist for longer durations during spaceflight, contributing to a 4–6 cm gain in stature—twice that observed on Earth during sleep [8]. Despite a multitude of studies of terrestrial mechanisms, the precise etiology of disc HNP following spaceflight remains unknown due to inherent study limitations and lack of spaceflight and post-flight recovery data.

The overall objective of this current study was to determine the influence of supraphysiologic swelling of the human lumbar disc on motion segment mechanics. This was accomplished by testing the hypotheses that supraphysiologic swelling and concomitant disc height changes cause: (1) increased bending stiffness and decreased ROM; (2) increased collagen fiber strains in the posterolateral annulus during flexion with compression; and (3) increased intradiscal pressure. The biomechanical responses of human cadaver lumbar motion segments were tested before and after swelling in physiologic saline to induce a range of disc height increases spanning the range reported for space flight.

Materials and methods

Specimen preparation

Human subjects committee approval was granted for in vitro tests of cadaveric human lumbar spines acquired through the UCSF willed body program. Eight fresh-frozen human lumbar segments (L2/3 or L4/5) from five donors (2 females, 3 males, age range 51–76) were thawed and cleaned of paraspinal musculature, while preserving bony, capsular, and ligamentous tissue. In each motion segment, the cranial and caudal vertebral bodies were individually embedded in urethane casting resin (Smooth-On, Easton, PA, USA) in such a way as to ensure a vertical spinal axis and permit unconstrained intervertebral motion. The caudal vertebral encasement was secured to a custom-designed test-rig base plate (Fig. 1). The cranial vertebra was fastened to one of two fixtures for the strain and flexibility tests.

Author Manuscript Author Manuscript Author Manuscript Author Manuscript

Protocol overview

Motion segments were thawed overnight and placed in a 4 °C saline bath for 2 h prior to testing to offset any differences in disc height upon fresh-freezing. Using fluoroscopy, disc height was calculated as the average of the posterior and anterior disc heights, and wedge angle was calculated as the angle formed by the superior and inferior endplates in the sagittal plane. Each specimen first underwent strain and flexibility tests (in randomized order) with unaltered disc hydration states. Between tests, specimens were replaced in the saline bath for 2 h to recover water loss during prior testing. After baseline flexibility and strain tests, each specimen was free-swelled in a 4 °C saline bath for between 40 and 93 h (mean 64.6 h) to achieve a range of hydration levels. Discs with a greater extent of degeneration were allowed to equilibrate for longer durations to account for degenerative variations in swelling pressure. Swelled specimens were imaged and re-tested according to the same protocol.

Strain testing

Each specimen underwent a combination of flexion and compression to impose eight postural configurations (Table 1). Compressive loads were chosen as fractions of torso weight (TW), where TW was 60 % of the estimated body weight above L3/L4 for our cadaveric sample demographic (400 N). We additionally adjusted the applied load for each sample so as to achieve an equivalent compressive stress (0.3 MPa), where individual disc cross sections were approximated as ellipses formed by the major and minor axes of the inferior endplate as measured via fluoroscopy (Table 2). Postural configurations 1–5 enabled quantification of axial compressibility, while configurations 7–8 mimicked loading combinations implicated in clinical cases of HNP. Postures were achieved using a custom jig (Fig. 1) comprising a set of four low-friction casters to dissipate longitudinal forces, an articulation plate, and a tilting vise (Walter Meier, La Vergne, TN, USA) in combination with a servo-hydraulic linear actuator (MTS Systems, Eden Prairie, MN, USA). Annular tissue strain was measured using 4 insect pins inserted into the posterolateral corner. Pin location was captured via photography and analyzed to calculate finite tissue strain [9], with a predicted maximum error of 3 % based on human input variability and the 1.5 megapixel camera resolution. Intradiscal pressure (IDP) was measured using a pressure-tip catheter (Gaeltec, Isle of Skye, Scotland) measuring 1.33 mm in diameter that was carefully inserted into the nucleus through the lateral aspect of the annulus and verified via X-ray. Each loading case was held for 30 s and data during the final 5 s were averaged.

Flexibility testing

Each specimen was subjected to non-constraining pure moment loads using a custom apparatus [10] comprising a system of pulleys, cables and a free-sliding base in combination with the servo-hydraulic linear actuator. Specimens were loaded in 2 Nm increments at 0.5 Nm/s to a maximum of 8 Nm for flexion and 6 Nm for extension, lateral bending, and axial rotation. Each moment increment was held for 30 s to allow for creep deformation. Vertebral three-dimensional kinematic response was measured using an optoelectronic motion-capture system (Northern Digital, Waterloo, Canada) and reported as Euler angles.

Author Manuscript Author Manuscript Author Manuscript Author Manuscript

Post-test analyses

After testing, specimens were removed from their resin encasement, cut through the mid-sagittal plane, and visually classified using the five-category degenerative Thompson grading scheme [11] according to gross morphological features (Grade 1 = healthy and non degenerated; Grade 5 = severely degenerated). Nucleus samples were then excised to quantify GAG content using the dimethylmethylene blue (DMMB) assay [12].

Insect pin locations at each load step were used to calculate the annular axial, circumferential, and shear components of the two-dimensional Lagrangian strain tensor, E, by examining changes in the distances and shear angles between pin pairs (Fig. 2). Strains were expressed relative to unloaded specimen strains in pre-swelled baseline tests. According to finite strain theory, the components of the strain tensor were calculated as:

$$E_{11}=\frac{1}{2}\left[\left(\frac{L_{11}}{L_{11_0}}\right)^2-1\right] \quad (1)$$

$$E_{22}=\frac{1}{2}\left[\left(\frac{L_{22}}{L_{22_0}}\right)^2-1\right] \quad (2)$$

$$E_{12}=\frac{1}{2}sin\,(-\Delta\theta)\left(\sqrt{1+2E_{11}}\,\sqrt{1+2E_{22}}\right) \quad (3)$$

Annular strain in the direction of collagen fibers (E_{fiber}) was determined as strain in the direction of the unit vector, **f**, which is aligned with the outer annulus fibers (Fig. 3):

$$E_{fiber}=f\cdot E=E_{11}\,cos^2\,\theta+E_{22}\,sin^2\,\theta+E_{12}\,sin\,\theta\,cos\,\theta \quad (4)$$

The ‘transition flexion angle’ (TFA) represents the flexion angle where E_{fiber} reaches 4 %, at which point the collagen deformation transitions from elastic to plastic and may induce tissue failure [13, 14]. ROM and stiffness were calculated in each principal direction; for bending flexibility, ROM was calculated as the Euler angular rotation of motion segments at the highest applied moment, relative to a neutral posture. For axial compressibility, ROM was calculated as the axial deflection under full TW application. Stiffness was calculated as the inverse slope of a trend line applied to the extensible zone of the load–response curve (Fig. 4).

All statistical analyses were performed using commercially available software (JMP, Version 7.0, SAS Institute Inc.). Pre- vs. post-swelling values were compared using paired one-tailed *t* tests. Linear regression analysis was performed for cases with continuous explanatory and response variables. Non-parametric ANOVA assessed differences in continuous variables

Author Manuscript Author Manuscript Author Manuscript Author Manuscript

among degeneration groups. Significance level was set at $p < 0.05$, while trends were defined when $0.05 < p < 0.1$. Grubbs' test for outliers was performed on potentially spurious data. Z values were calculated as the difference between the outlier and the mean divided by the standard deviation, and compared to tabulated critical Z values.

Results

Post-swelling changes in measured properties are provided in Table 2. Disc height was significantly increased post-swelling ($p < 0.001$). The extent of hydration was represented by the increase in disc height (DH %) from baseline to swelled states, and ranged by specimen from 4 to 23 %, mean 14.2 %. Stiffness in flexion, lateral bending, and axial rotation were significantly increased post-swelling ($p < 0.05$), while ROM in flexion, lateral bending, and axial rotation were significantly reduced ($p < 0.05$). Extension stiffness and ROM were unchanged. E_{fiber} under TW + 7° flexion and TW + 10° flexion, and IDP in neutral posture, under TW, under TW + 3° flexion, under TW + 7° flexion, and under 8 Nm pure flexion were all significantly increased post-swelling ($p < 0.05$). TFA and wedge angle were significantly reduced post-swelling ($p < 0.05$ and $p < 0.001$, respectively).

Post-swelling changes in bending flexibility correlated with DH % to different degrees depending on testing direction. Stiffening in flexion was significantly correlated with DH % ($R^2 = 0.70$, $p = 0.01$; Fig. 5a); consistent with this, flexion ROM negatively correlated with DH % ($R^2 = 0.54$, $p = 0.04$; Fig. 5b). Lateral bending ROM varied positively with DH % as a trend ($R^2 = 0.41$, $p = 0.09$).

Increases in DH % led to increases in E_{fiber} under various testing conditions. When subjected to TW plus 3° flexion, E_{fiber} correlated positively with DH % as a trend ($R^2 = 0.40$, $p = 0.09$). This swelling-induced increase in surface strain became more pronounced with greater degrees of flexion. Under TW plus 7° flexion, E_{fiber} correlated positively with DH % ($R^2 = 0.58$, $p = 0.03$; Fig. 5c). However, under TW plus 10° flexion, E_{fiber} and DH % were not significantly correlated. Variation in DH % did not explain variation in changes in E_{fiber} under TW loading without flexion ($R^2 < 0.15$, $p > 0.1$). The relationship between E_{fiber} and flexion angle was well described by a second-order polynomial, which was used to predict specimen TFA. TFA decreased with swelling and correlated negatively with DH % ($R^2 = 0.41$, $p = 0.09$; Fig. 5d). A graphical interpretation of shifts in TFA is provided (Fig. 6).

Changes in IDP under TW plus 7° of flexion contained one outlier as detected by the Grubbs' test for outliers ($Z = 2.436$). With this outlier removed, IDP under TW plus 7° of flexion correlated positively with DH % ($R^2 = 0.77$, $p = 0.009$, $N = 7$; Fig. 5e). With the outlier included, this correlation was not significant ($R^2 = 0.11$, $p = 0.3990$, $N = 7$; Fig. 5e). IDP under TW plus 3° and 10° of flexion correlated positively with DH % as trends. Under pure moment flexion (no compression), IDP correlated positively with DH % ($R^2 = 0.59$, $p = 0.03$; Fig. 5f).

Motion segments straightened with disc height as indicated by loss of disc wedge angle ($R^2 = 0.27$, $p = 0.04$; Fig. 5g) and a greater increase in posterior than anterior disc height (17 vs.

Author Manuscript Author Manuscript Author Manuscript Author Manuscript

5 %, $p = 0.04$). The loss of disc wedge angle led to decreased ROM in flexion ($R^2 = 0.94$, $p < 0.0001$; Fig. 5h) and decreased stiffening in extension ($R^2 = 0.65$, $p = 0.04$; Fig. 5i). No significant correlations were found for extension ROM and flexion stiffness with wedge angle. None of the specimens in the current study had a Thompson degeneration grade 1 or 2. Proteoglycan content within the nucleus was 100.3 % greater in grade 3 specimens ($N = 4$; 6.64 % dry weight) than in grade 5 specimens ($N = 5$; 3.31 % dry weight, $p = 0.0146$).

Discussion

The results of this cadaveric study indicate that swelling-induced disc height increases (comparable to those reported for long-duration space flight) stiffen the spine and elevate annular strain and nuclear pressure during forward bending. Given the vital role of the annulus in the localization of nuclear material and prevention of HNP [16], these significant strain and pressure increases may help explain elevated HNP rates post-flight. While prior studies have shown correlations between hydration of excised annulus tissue and annulus tensile properties [22–24], this is the first whole-disc experiment linking disc swelling with changes in motion segment biomechanics and disc tissue pressure and strain. We also extend upon prior work conducted on the effect of diurnal disc height fluctuations on biomechanics to include disc height increases likely experienced during spaceflight. Given that astronauts experience a stature gain that is twice that observed during bed rest [8], we may expect disc height increases to similarly be about twice those observed during bed rest. Head-down tilt bed rest increases disc height by 0–10 % [29], and thus our disc height increases of 4–23 % are relevant for expected values during spaceflight. Furthermore, the biomechanical trends we identified by varying disc height may be incorporated into future spine models. Findings from this study may also be relevant for non-astronauts by providing insight into increased lumbar stiffness and risk of injury in the morning after overnight disc swelling [6].

Forward bending is implicated in HNP, and we observed a positive correlation between DH % and both increased stiffness and decreased ROM in flexion, likely due to axial pre-strain in the annulus and paraspinal ligaments. We also observed large strain increases with increased disc height when each herniation posture was considered separately. As a general rule, a ~50 % increase in E_{fiber} was observed in flexed/compressed motion segments with 15–20 % disc height increases. Furthermore, the elastic limit of fibers was reached earlier under supraphysiologic swelling conditions, as indicated by decreased TFA. These results suggest that post-flight astronauts may be more likely to strain their annular collagen fibers past the elastic limit than the general population performing the same activities, thus accelerating accumulation of tissue damage and increasing failure risk. The highest fiber strains during physiologic movement occur in the posterolateral annulus [17, 18], so tissue failure may initiate in this region via plastic deformation of fibers repeatedly stretched beyond their elastic limits.

It should be noted that the discs may have swelled past physiologic values during the 2 h of pre-swelling due to the absence of load, and thus the pre-swelled ‘baseline’ condition does not necessarily represent an in vivo condition. However, we report all data as ratios, and pre-swelled baseline data for ROM in flexion (6.4° ± 2.2°) and lateral bending (3.4° ± 1.8°), E_{fiber} under 7° flexion (3.1 ± 1.5 %), and average TFA (8.3°) all fell within previously

Author Manuscript Author Manuscript Author Manuscript Author Manuscript

reported ranges [17–19]. The 2 h free-swell time we allowed between strain and flexibility tests was likely sufficient to recover water loss based on prior studies. For example, Dhillon and coworkers applied a 1 MPa stress for 20 min and found that disc height had begun to plateau after a 40-min recovery time [15]. In our study, the applied loads were much smaller (less than 0.5 MPa) and were held for only 30 s; thus, we are confident that a 2 h recovery time was sufficient.

Our results show an increase in IDP with disc swelling under flexion and compression. Pre-swelled baseline IDP data compared well with in vitro and in silico studies [20, 21]. Generation of abnormally high nuclear pressures may facilitate migration of nuclear material through strained annular layers.

Numerous bed rest studies have reported decreased lumbar lordosis following bed rest [25, 26], while others have reported increased or unchanged lordosis [29, 31]. We observed a loss of disc wedging angle with increased swelling, indicating a straightening of the spine. Lumbar lordosis is influenced by upper body weight [27] and thus may not be maintained in microgravity conditions. Loss of lordosis presumably adds an additional pre-strain on the posterior annulus and may contribute to the measured decrease in flexion ROM. These lordosis changes contribute to overall spinal lengthening, and may play a part in the increased herniation risk following spaceflight.

Despite its novel features, the current work has a number of limitations inherent to cadaveric studies. The most important limitation was a challenge in accurately representing muscle-derived constraints. Postural musculature provides a protective factor against exceeding flexion limit [28] and is known to atrophy during space flight and bed rest [26]. To isolate the effect of swelling on bending stiffness, we used a pure moment testing protocol such that the loading boundary conditions remain equivalent between tests [33]. To assess the effect of swelling on annular strain and nucleus pressure, we utilized a second testing protocol that compressed the specimens while they were constrained to set flexed positions [4]. This second test more closely mimics lifting in a flexed posture with active trunk muscles. However, the compressive stresses applied in this second test are relatively low (0.3 MPa) compared to those recorded in vivo during activities of daily living (0.5 to 1.8 MPa for activities in upright postures) [30]. Another limitation is the small sample size and accompanying low statistical power for detecting significant correlations. This precluded a more thorough investigation of age-dependent herniation risk. We were able to observe clear trends, but larger studies may help verify the current findings. Lastly, we did not test specimens from the cervical spine, in which post-spaceflight herniation risk is even more markedly increased than in the lumbar spine [1]. In general, there is a lack of post-spaceflight data for the cervical spine, and future studies should address this need. Notwithstanding these shortcomings, we observed signifi-cant relationships between disc swelling and factors associated with injury risk (nucleus pressure and annular strain) that highlight potential causal relationships between microgravity exposure and post-flight back pain and disc herniation.

In conclusion, we observed that swelling-induced increases in disc height led to increases in annular strain and nuclear pressure during spinal movement, suggesting that individualized

Author Manuscript Author Manuscript Author Manuscript Author Manuscript

measures of DH % (obtainable by ultrasound in space [8]) provide insight into herniation risk. Our data suggest that astronauts should limit flexion activities upon returning to Earth until re-acclimation to gravity loading so as to prevent overloading tissue that is already susceptible to damage accumulation and HNP. Increased disc height, disc volume, and intervertebral length following 21 and 60 days of bed rest do not return to pre-bed rest values until at least 5 months and 2 years later, respectively [29, 32]. This suggests that astronauts may expect the biomechanical changes observed in our study to persist for months or years following spaceflight, and the recovery time may depend on mission duration. HNP risk also varies by disc quality, suggesting that DH % could be used as an indicator for when crew may safely resume unrestricted activities post-flight. Finally, by demonstrating relationships between DH %, posture, spine stiffness, and disc pressure/strain, this current study may help to develop countermeasures for mitigating deleterious microgravity-induced changes and optimizing post-flight reconditioning protocols.

Acknowledgments

This work was supported by the National Aeronautics and Space Administration (NASA), Grants NNX10AM18G and NNX13AM89G.

References

1. Johnston SL, Campbell MR, Scheuring R, Feiveson AH. Risk of herniated nucleus pulposus among US astronauts. Aviat Space Environ Med. 2010; 81:566–574. doi:10.3357/ASEM.2427.2010. [PubMed: 20540448]
2. Mirza SK, White AA III. Anatomy of intervertebral disc and pathophysiology of herniated disc disease. J Clin Laser Med Surg. 1995; 13:131–142. doi:10.1089/clm.1995.13.131. [PubMed: 10150636]
3. Simunic DI, Robertson PA, Broom ND. Mechanically induced disruption of the healthy bovine intervertebral disc. Spine. 2004; 29:972–978. [PubMed: 15105667]
4. Adams MA, Hutton WC. Prolapsed intervertebral disc: a hyperflexion injury. Spine. 1982; 7:184–191. [PubMed: 7112236]
5. Veres SP, Robertson PA, Broom ND. The morphology of acute disc herniation: a clinically relevant model defining the role of flexion. Spine. 2009; 34:2288–2296. doi:10.1097/BRS.0b013e3181a49d7e. [PubMed: 19934808]
6. Malko JA, Hutton WC, Fajman WA. An in vivo magnetic resonance imaging study of changes in the volume (and fluid content) of the lumbar intervertebral discs during a simulated diurnal load cycle. Spine. 1999; 24:1015–1022. doi:10.1097/00007632-199905150-00016. [PubMed: 10332795]
7. Adams MA, Dolan P, Hutton WC. Diurnal variations in the stresses on the lumbar spine. Spine. 1987; 12:130–137. doi:10.1097/00007632-198703000-00008. [PubMed: 3589804]
8. Wing PC, Tsang IK, Susak L, Gagnon F, Gagnon R, Potts JE. Back pain and spinal changes in microgravity. Orthop Clin North Am. 1991; 22:255–262. [PubMed: 1826549]
9. Cassidy JJ, Hiltner A, Baer E. Hierarchical structure of the intervertebral disc. Connect Tissue Res. 1989; 23:75–88. doi:10.3109/03008208909103905. [PubMed: 2632144]
10. Eguizabal J, Tufaga M, Scheer JK, Ames C, Lotz JC, Buckley JM. Pure moment testing for spinal biomechanics applications: fixed versus sliding ring cable-driven test designs. J Biomech. 2010; 43:1422–1425. doi:10.1016/j.jbiomech. 2010.02.004. [PubMed: 20181340]
11. Thompson JP, Pearce RH, Schechter MT, Adams ME, Tsang IKY, Bishop PB. Preliminary evaluation of a scheme for grading the gross morphology of the human intervertebral disc. Spine. 1990; 15:411–415. doi:10.1097/00007632-199005000-00012. [PubMed: 2363069]

Author Manuscript Author Manuscript Author Manuscript Author Manuscript

12. Farndale RW, Sayers CA, Barrett AJ. A direct spec-trophotometric microassay for sulfated glycosaminoglycans in cartilage cultures. Connect Tissue Res. 1982; 9:247–248. doi: 10.3109/03008208209160269. [PubMed: 6215207]
13. Harkness, RD. Treatise on Collagen. Vol. 2. Academic Press; London: 1968. Mechanical properties of collagenous tissues..
14. Hickey DS, Hukins DW. Relation between the structure of the annulus fibrosus and the function and failure of the inter-vertebral disc. Spine. 1980; 5:106–116. [PubMed: 6446156]
15. Dhillon N, Bass EC, Lotz JC. Effect of frozen storage on the creep behavior of human intervertebral discs. Spine. 2001; 26:883–888. [PubMed: 11317110]
16. Paul Brinckmann D. Injury of the annulus fibrosus and disc protrusions: an in vitro investigation on human lumbar discs. Spine. 1986; 11:149–153. doi:10.1097/00007632-198603000-00009. [PubMed: 3704801]
17. Stokes IA. Surface strain on human intervertebral discs. J Orthop Res. 1987; 5:348–355. doi: 10.1016/0021-9290(86)90034-5. [PubMed: 3625358]
18. Shiraz-Adl A. Strain in fibers of a lumbar disc: analysis of the role of lifting in producing disc prolapse. Spine. 1989; 14:96–103. [PubMed: 2913676]
19. Yamamoto I, Panjabi MM, Crisco T, Oxland TOM. Three-dimensional movements of the whole lumbar spine and lumbosacral joint. Spine. 1989; 14:1256–1260. doi: 10.1097/00007632-198911000-00020. [PubMed: 2603060]
20. Adams MA, McNally DS, Wagstaff J, Goodship AE. Abnormal stress concentrations in lumbar intervertebral discs following damage to the vertebral bodies: a cause of disc failure? Eur Spine J. 1993; 1:214–221. doi:10.1007/BF00298362. [PubMed: 20054920]
21. Steffen T, Baramki HG, Rubin R, Antoniou J, Aebi M. Lumbar intradiscal pressure measured in the anterior and posterolateral annular regions during asymmetrical loading. Clin Biomech. 1998; 13:495–505. doi:10.1016/S0268-0033(98)00039-4.
22. Panagiotacopulos ND, Pope MH, Bloch R, Krag MH. Water content in human intervertebral discs: part II. viscoelastic behavior. Spine. 1987; 12:918–924. [PubMed: 3441838]
23. Hirsch C, Galante J. Laboratory conditions for tensile tests in annulus fibrosus from human intervertebral discs. Acta Orthop Scandinav. 1967; 38:148–162. [PubMed: 6033410]
24. Skaggs DL, Weidenbaum M, Ratcliffe A, Mow VC. Regional variation in tensile properties and biochemical composition of the human lumbar anulus fibrosus. Spine. 1994; 19:1310–1319. doi: 10.1097/00007632-199406000-00002. [PubMed: 8066509]
25. Cao P, Kimura S, Macias BR, Ueno T, Watenpaugh DE, Hargens AR. Exercise within lower body negative pressure partially counteracts lumbar spine deconditioning associated with 28-day bed rest. J Appl Physiol. 2005; 99:39–44. doi:10.1152/japplphysiol.01400.2004. [PubMed: 15761083]
26. Belavý DL, Armbrecht G, Gast U, Richardson CA, Hides JA, Felsenberg D. Countermeasures against lumbar spine deconditioning in prolonged bed rest: resistive exercise with and without whole body vibration. J Appl Physiol. 2010; 109:1801–1811. doi:10.1097/BRS. 0b013e3181cc93e8. [PubMed: 20864564]
27. Whitcome KK, Shapiro LJ, Lieberman DE. Fetal load and the evolution of lumbar lordosis in bipedal hominins. Nature. 2007; 450:1075–1078. doi:10.1038/nature06342. [PubMed: 18075592]
28. Adams MA, Hutton WC. Has the lumbar spine a margin of safety in forward bending? Clin Biomech. 1986; 1:3–6. doi:10.1016/0268-0033(86)90028-8.
29. Belavý DL, Bansmann PM, Böhme G, Frings-Meuthen P, Heer M, Rittweger J, Zange J, Felsenberg D. Changes in intervertebral disc morphology persist 5 mo after 21-day bed rest. J Appl Physiol. 2011; 111:1304–1314. doi:10.1152/japplphysiol.00695.2011. [PubMed: 21799122]
30. Wilke HJ, Neef P, Caimi M, Hoogland T, Claes LE. New in vivo measurements of pressures in the intervertebral disc in daily life. Spine. 1999; 24:755–762. doi: 10.1097/00007632-199904150-00005. [PubMed: 10222525]
31. Belavý DL, Ohshima H, Bareille MP, Rittweger J, Felsenberg D. Limited effect of fly-wheel and spinal mobilization exercise countermeasures on lumbar spine deconditioning during 90d bed-rest in the Toulouse LTBR study. Acta Astronaut. 2011; 69:406–419. doi:10.1016/j.actaastro. 2011.05.015.

Author Manuscript Author Manuscript Author Manuscript Author Manuscript

32. Belavý DL, Armbrecht G, Felsenberg D. Incomplete recovery of lumbar intervertebral discs 2 years after 60-day bed rest. Spine. 2012; 37:1245–1251. doi:10.1097/BRS.0b013e3182354d84. [PubMed: 21971124]

33. Panjabi MM. Biomechanical evaluation of spinal fixation devices: I. A conceptual framework. Spine. 1988; 13:1129–1134. [PubMed: 3206270]

Author Manuscript Author Manuscript Author Manuscript Author Manuscript

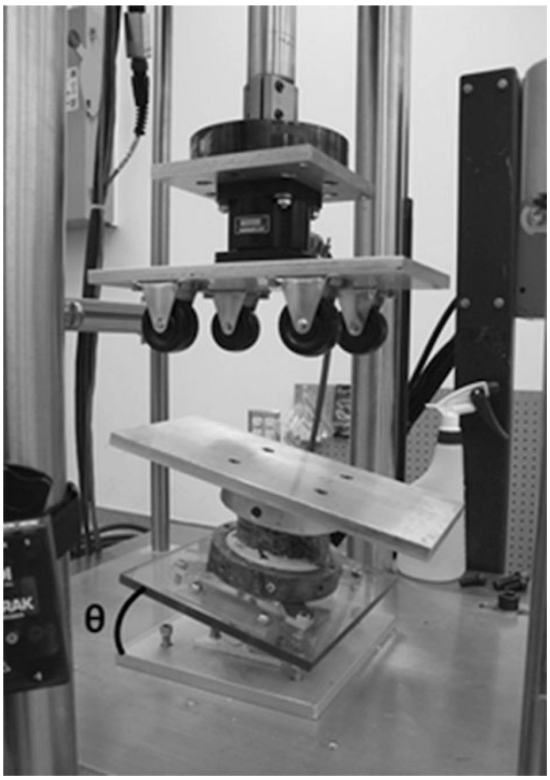

Fig. 1.

Image of custom jig to impose postures implicated in disc herniation on motion segments. Linear actuator lowers and each of four caster rollers make contact with plate sitting atop motion segment (positioned with anterior side on the *left* in this image) to impose compression and flexion angle, θ

Author Manuscript Author Manuscript Author Manuscript Author Manuscript

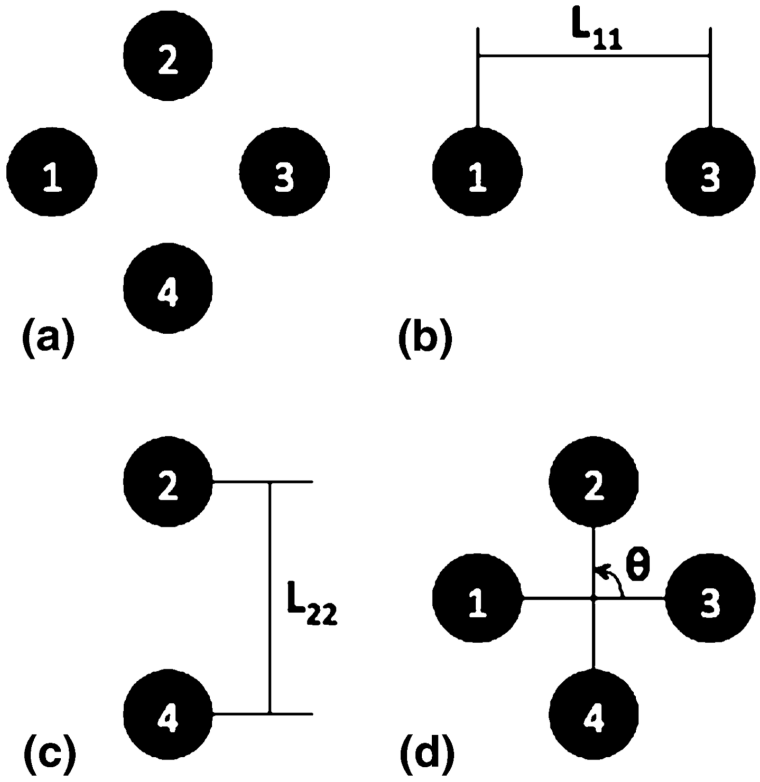

Fig. 2.

a Idealized 4-point grid; **b** horizontal distance (L_{11}) between points 1 and 3 used to calculate E_{11}; **c** vertical distance (L_{22}) between points 2 and 4 used to calculate E_{22}; **d** definition of shear angle θ

Author Manuscript Author Manuscript Author Manuscript Author Manuscript

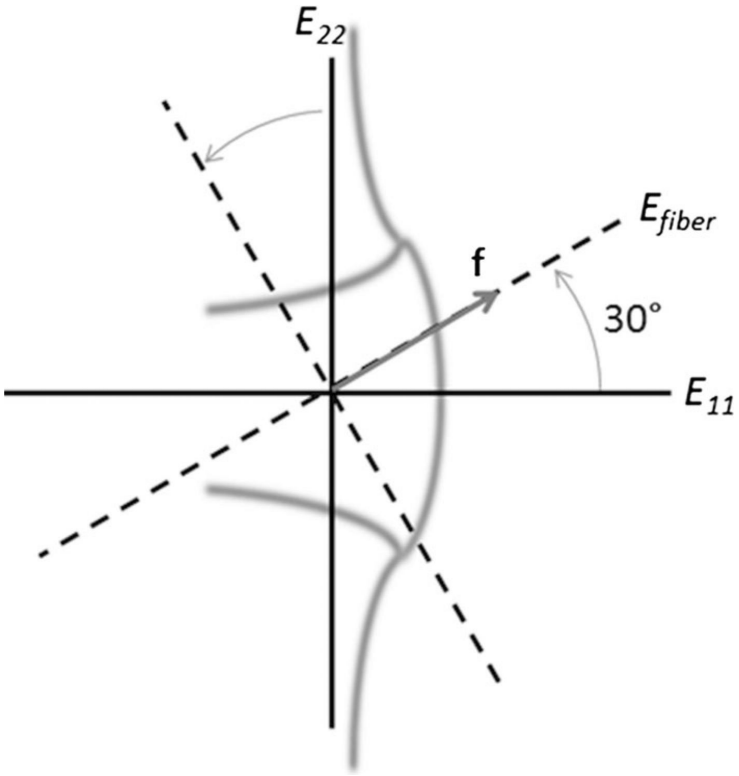

Fig. 3.

Schematic of motion segment and superimposed Cartesian coordinate system whose origin represents location of strain measurement. Coordinate system transformation of 30° is applied to determine tissue strain in the direction of collagen fibers

Author Manuscript Author Manuscript Author Manuscript Author Manuscript

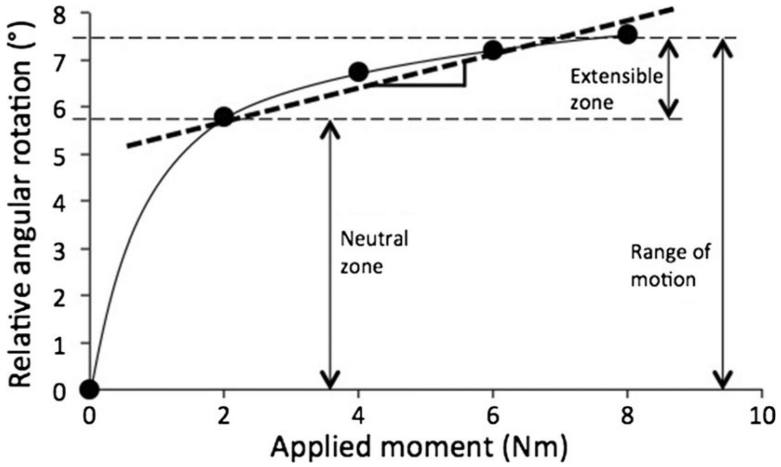

Fig. 4.

Nonlinear moment–response curve for Specimen 1 showing joint stiffening as physiologic loads increase. The neutral zone was defined as the region of the *curve* from 0 to 2 Nm applied moment. Range of motion was calculated as the angular rotation of motion segments at the highest applied moment. Stiffness was calculated as the inverse slope of a trend line (*thick dashed line*) applied to the extensible zone

Author Manuscript
Author Manuscript
Author Manuscript
Author Manuscript

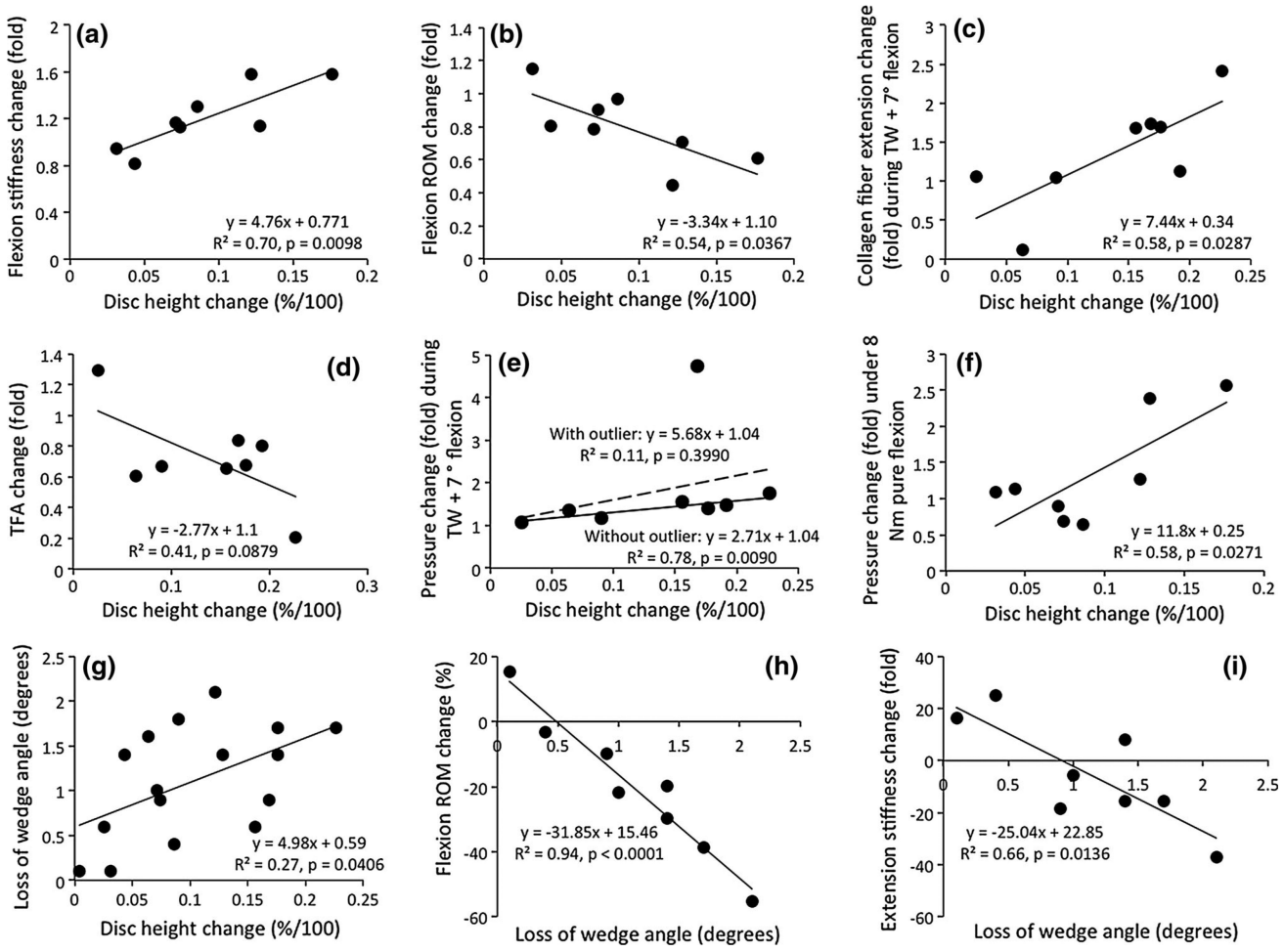

Fig. 5.

Post-swelling fold changes in **a** flexion stiffness, **b** flexion ROM, **c** E_{fiber} after swelling for specimen subjected to TW plus 7° flexion, **d** transition flexion angle, **e** pressure change during TW plus 7° flexion both with and without inclusion of outlier, **f** pressure change under 8 Nm pure flexion, and **g** loss of wedge angle with increasing disc height change; post-swelling changes in **h** flexion ROM and **i** extension stiffness with loss of disc wedge angle

Author Manuscript Author Manuscript Author Manuscript Author Manuscript

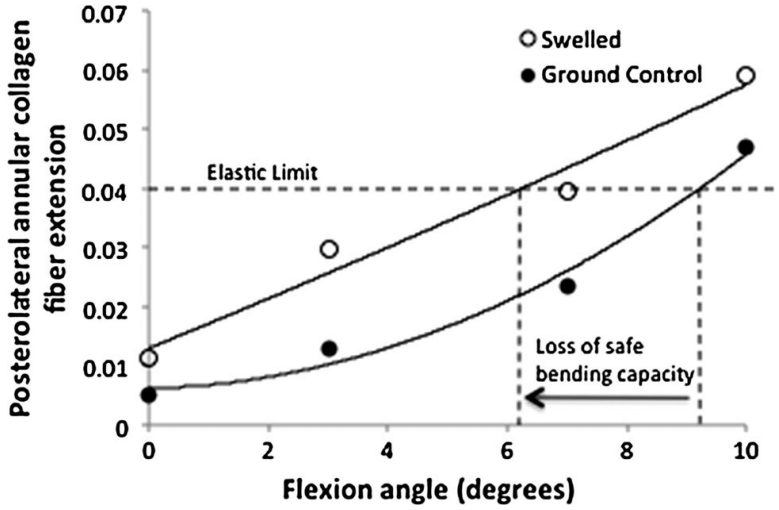

Fig. 6.

Example of left-ward shifting of curve fit from a 17.6 % increase in disc height. Transition flexion angle is decreased from 9.2° to 6.3° in this case

Author Manuscript

Author Manuscript

Author Manuscript

Author Manuscript

Table 1

Postural configurations for strain and axial compressibility tests

Postural configuration	Flexion angle (°)	Compressive load
1	0	0
2	0	¼ TW
3	0	½ TW
4	0	¾ TW
5	0	TW
6	3	TW
7	7	TW
8	10	TW

TW represents estimated average torso weight adjusted by disc cross-sectional area to achieve 0.3 MPa compressive stress

Author Manuscript Author Manuscript Author Manuscript Author Manuscript

Table 2

Specimen characteristics, disc swell time, and post-swelling changes in measured variables

Specimen	**1**	**2**	**3**	**4**	**5**	**6**	**7**	**8**	**Avg.**	**SD**	***p* value**
Gender	M	M	M	F	F	M	M	M	-	-	-
Age	52	51	76	65	74	52	51	76	*62*	*12*	-
Spinal level	L2/3	L2/3	L2/3	L2/3	L2/3	L4/5	L4/5	L4/5	-	-	-
Vertebral area (mm^2)	1450	1720	1580	1135	1593	1693	1383	1998	*1569*	*256*	-
Torso weight plus muscle activation (*N*)	443.4	472.2	433.7	311.7	437.4	464.7	379.7	584.4	*436.4*	*74.3*	-
Degeneration grade	3	3	3	3	5	4	5	5	*4*	*1*	-
Proteoglycan content (% dry wt.)	6.84	6.33	7.65	5.72	5.15	6.21	2.41	2.38	*5.34*	*1.96*	-
Disc swell time (h)	40.0	69.4	50.0	48.0	90.0	64.0	93.0	62.3	*64.6*	*19.2*	-
Disc ht. % increase (strain tests)	22.7	6.4	9.0	15.6	2.5	19.2	17.6	16.8	*13.7*	*7.0*	*0.0001**
Disc ht. % increase (flexibility tests)	3.1	7.1	12.2	4.3	7.4	12.8	8.6	17.6	*9.1*	*4.8*	*0.001**
Disc ht. % increase (effective)	22.6	7.1	14.3	4.4	7.4	19.2	18.2	20.0	*14.2*	*6.9*	*0.0002**
Flexion stiffness change (fold)	0.95	1.16	1.58	0.81	1.13	1.14	1.30	1.58	*1.21*	*0.27*	*0.048**
Flexion ROM change (fold)	1.15	0.78	0.45	0.80	0.90	0.70	0.97	0.61	*0.80*	*0.22*	*0.023**
Extension stiffness change (fold)	1.16	0.94	0.63	0.85	0.82	1.08	1.25	0.84	*0.95*	*0.20*	*0.287*
Extension ROM change (fold)	2.19	0.95	0.98	1.01	1.05	0.99	0.78	0.82	*1.10*	*0.45*	*0.377*
Lateral bending stiffness change (fold)	0.65	1.02	1.43	1.59	2.01	1.88	1.56	1.94	*1.51*	*0.47*	*0.011**
Lateral bending ROM change (fold)	1.16	0.98	0.60	0.83	0.47	0.40	0.51	0.59	*0.69*	*0.27*	*0.030**
Axial rotation stiffness change (fold)	1.72	1.25	1.81	2.19	1.41	1.10	1.69	2.46	*1.70*	*0.46*	*0.001**
Axial rotation ROM change (fold)	0.55	0.71	0.65	1.01	0.76	0.83	0.70	0.42	*0.70*	*0.18*	*0.019**
Annular surface strain under TW + 7° flexion (fold)	2.42	0.12	1.04	1.68	1.05	1.13	1.69	1.74	*1.36*	*0.68*	*0.011**
Annular surface strain under TW + 10° flexion (fold)	1.99	0.13	1.83	1.27	1.24	1.33	1.26	1.93	*1.37*	*0.59*	*0.003**
TFA change (fold)	0.21	0.60	0.67	0.66	1.30	0.81	0.68	0.84	*0.72*	*0.30*	*0.027**
Pressure change in neutral posture (fold)	2.03	1.30	2.11	1.17	1.10	2.25	1.55	2.19	*1.71*	*0.48*	*0.002**
Pressure change under TW (fold)	1.36	1.10	1.44	1.06	1.03	1.31	1.19	1.18	*1.21*	*0.15*	*0.005**

Eur Spine J. Author manuscript; available in PMC 2017 September 01.

Author Manuscript Author Manuscript Author Manuscript Author Manuscript

Specimen	1	2	3	4	5	6	7	8	Avg.	SD	*p* value
Pressure change under TW + 3° flexion (fold)	1.68	1.06	1.18	1.26	1.24	1.22	1.42	4.29	*1.67*	*1.07*	*0.045**
Pressure change under TW + 7° flexion (fold)	1.75	1.36	1.17	1.55	1.07	1.48	1.41	4.74[a]	*1.81*	*1.20*	*0.027**
Pressure change under 8 Nm pure flexion (fold)	1.08	0.90	1.27	1.13	0.68	2.39	0.64	2.57	*1.33*	*0.74*	*0.265*
Loss of wedge angle pre-PM testing (°)	0.1	1	2.1	1.4	0.9	1.4	0.4	1.7	*1.1*	*0.7*	*0.001**
Loss of wedge angle pre-HNP testing (°)	1.7	1.6	1.8	0.6	0.6	0.1	1.4	0.9	*1.1*	*0.6*	*0.0009**

Note that two disc height increases were measured, and represent the changes between baseline and swelled heights measured just before (1) strain or (2) flexibility testing. The effective disc height increase represents the increase from immediately pre-swelling to immediately post-swelling. Only mechanical properties with significant pre- vs. post-swelling changes or correlations to disc height are shown. Data Summary Statistics are italicized. *p* values are for paired *t* tests comparing pre- vs. post-swelling raw values for each variable

* $p < 0.05$

[a] This pressure data point was removed as an outlier

Eur Spine J. Author manuscript; available in PMC 2017 September 01.